20

Statistical Errors in Remote Passive Wireless SAW Sensing Employing Phase Differences

Y.S. Shmaliy, O.Y. Shmaliy, O. Ibarra-Manzano,
J. Andrade-Lucio, and G. Cerda-Villafana
Electronics Department, Guanajuato University
Mexico

1. Introduction

Passive remote wireless sensing employing properties of the surface acoustic wave (SAW) has gained currency during a couple of decades to measure different physical quantities such as temperature, force (pressure, torque, and stress), velocity, direction of motion, etc. with a resolution of about 1% [1]. The basic principle utilized in such a technique combines advantages of the precise piezoelectric sensors [2, 3, 4], high SAW sensitivity to the environment, passive (without a power supply) operation, and wireless communication between the sensor element and the reader (interrogator). Several passive wireless SAW devices have been manufactured to measure temperature [1], identify the railway vehicle at high speed [5], and pressure and torque [6].

The information bearer in such sensors is primarily the time delay of the SAW or the central frequency of the SAW device. Most passive SAW sensors are designed as reflective delay lines with M reflectors[1] and operate as sketched in Fig. 1. At some time instant $t_0 = 0$, the reader transmits the electromagnetic wave as an interrogating radio frequency (RF) pulse ($K = 1$), pulse burst ($K > 1$), pulse train, or periodic pulse burst train. The interdigital transducer (IDT) converts the electric signal to SAW, and about half of its energy distributes to the reflector. The SAW propagates on the piezoelectric crystal surface with a velocity v through double distances ($2L_1$ and $2L_2$), attenuates (6 dB per μs delay time [5]), reflects partly from the reflectors (R_1 and R_2), and returns back to the IDT. Inherently, the SAW undergoes phase delays on the piezoelectric surface. The returned SAW is reconverted by the IDT to the electric signal, and retransmitted to the interrogator. While propagating, the RF pulse decays that can be accompanied with effects of fading. At last, K pairs of RF pulses (Fig. 1b) appear at the coherent receiver, where they are contaminated by noise. In these pulses, each inter distance time delay $\Delta\tau_{(2k)(2k-1)} = 2(L_2 - L_1)/v$, $k \in [1,K]$, bears information about the measured quantity, i.e., temperature [1], pressure and torque [5], vehicle at high speed [6], etc.

To measure $\Delta\tau_{(2k)(2k-1)}$, a coherent receiver is commonly used [7], implementing the maximum likelihood function approach. Here, the estimate of the RF pulse phase relative to the reference is formed to range either from $-\pi/2$ to $\pi/2$ or from $-\pi$ to π by, respectively,

[1] Below, we consider the case of $M = 2$.

Source: Acoustic Waves, Book edited by: Don W. Dissanayake,
ISBN 978-953-307-111-4, pp. 466, September 2010, Sciyo, Croatia, downloaded from SCIYO.COM

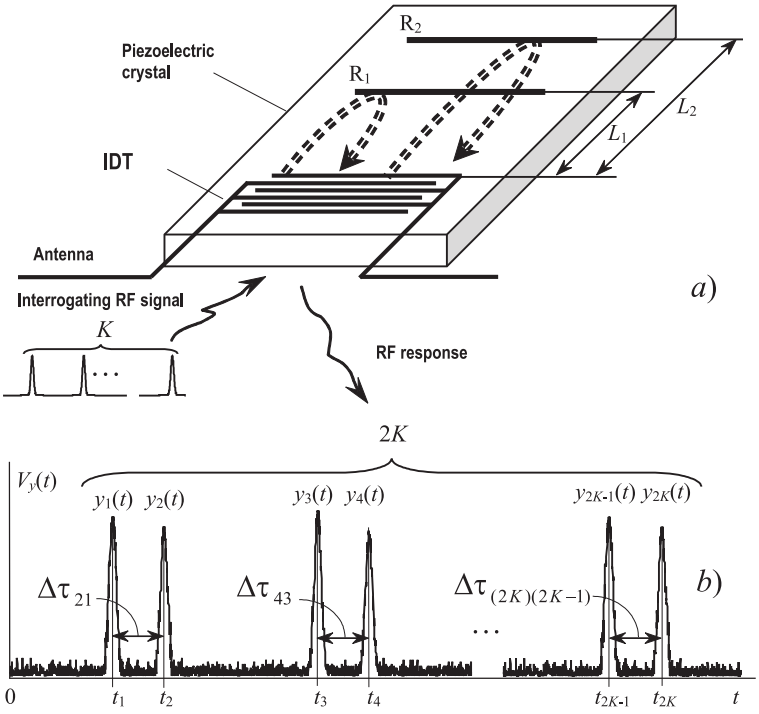

Fig. 1. Operational principle of remote SAW sensing with phase measurement: a) basic design of passive SAW sensors and b) reflected pulses at the coherent receiver detector [25].

$$\hat{\theta} = \arctan\frac{Q}{I}, \tag{1}$$

$$\hat{\theta} = \begin{cases} \arctan(Q/I), & I \geq 0 \\ \arctan(Q/I) \pm \pi, & I < 0, \begin{cases} Q \geq 0 \\ Q < 0 \end{cases} \end{cases}, \tag{2}$$

where I and Q are the in-phase and quadrature phase components obtained for the received pulse. With differential phase measurement (DPM), the phase difference in every pair of pulses is calculated by

$$\hat{\Theta}_k = \hat{\theta}_{2k} - \hat{\theta}_{2k-1} \tag{3}$$

and used as a current DPM. Here several estimates may be averaged to increase the signal-to-noise ratio (SNR) [7]. Averaging works out efficiently if the mean values are equal. Otherwise, the differential phase diversity is of interest to estimate either the vehicle's velocity (Doppler shift) or the random error via

$$\hat{\Psi}_k = \hat{\Theta}_k - \hat{\Theta}_{k-1}. \tag{4}$$

An accurate estimate $\hat{\Theta}_k$ is a principal goal of the receiver. To obtain it with a permitted inaccuracy in the presence of noise, the interrogating signal must be transmitted with a sufficient peak power that, however, should not be redundant. The peak power is coupled with the SNR. Therefore, statistical properties of $\hat{\Theta}_k$ and $\hat{\Psi}_k$ are of prime interest. Knowing these properties and the peak power of the interrogating pulse, one can predict the measurement error and optimize the system. In this Chapter, we discuss limiting and approximate statistical errors in the estimates (3) and (4).

2. Signal model

For SAW sensors with identification marks, the readers are often designed to interrogate the sensors with a linear frequency modulated (LFM) RF impulse request signal [8, 9]

$$x(t) = \sqrt{2S}a(t)\cos\left(2\pi f_0 t + \frac{\alpha t^2}{2} + \theta_0\right), \tag{5}$$

where $2S$ and θ_0 are the peak-power and initial phase, respectively, f_0 is the initial carrier frequency, and t is the current time. The LFM pulse can have a near rectangular normalized waveform $a(t)$ of duration T such that $\alpha = \Delta\omega/T$, where $\Delta\omega$ is a required angular frequency deviation, overlapping all the sensor responses.

It turns out that noise does not perturb $x(t)$ substantially in the sensor. Therefore, assuming Gaussian envelope in the reflected pulses, the induced SAW reflected from the reflectors R_1 and R_2 and then reconverted and retransmitted can be modeled with, respectively,

$$\begin{aligned} s_1(t) &= \sum_{k=1}^{K} u_{2k-1}(t) \\ &= \sqrt{2S}\sum_{k=1}^{K} \beta_{2k-1}(t) e^{-b^2(t-t_{2k-1})^2} \cos[2\pi f_{2k-1} t + \vartheta_{2k-1}(t)], \end{aligned} \tag{6}$$

$$\begin{aligned} s_2(t) &= \sum_{k=1}^{K} u_{2k}(t) \\ &= \sqrt{2S}\sum_{k=1}^{K} \beta_{2k}(t) e^{-b^2(t-t_{2k})^2} \cos[2\pi f_{2k} t + \vartheta_{2k}(t)], \end{aligned} \tag{7}$$

where $\beta_i^2(t)$, $i \in [1, 2K]$, is a normalized instantaneous power caused by attenuation and fading. The full phase shifts relative to the carrier and its constituent induced during the SAW propagation are given by, respectively,

$$\vartheta_{2k-1} = \phi_{2k-1} - \psi_{2k-1} + \theta_0, \tag{8}$$

$$\vartheta_{2k} = \phi_{2k} - \psi_{2k} + \theta_0, \tag{9}$$

where $k \in [1, K]$, ϕ_{2k-1} and ϕ_{2k} are phase shifts caused by various reasons, e.g., RF wave propagation, Doppler effect, frequency shift between the signals, etc. Here, the relevant information bearing phase shifts can be evaluated with, respectively,

$$\psi_{2k-1} = 4\pi f_{2k-1}\frac{L_1}{v} \quad \text{and} \quad \psi_{2k} = 4\pi f_{2k}\frac{L_2}{v}. \tag{10}$$

At the receiver, each of the RF pulses $u_i(t)$, $i \in [1, 2K]$, is contaminated by zero mean additive stationary narrowband Gaussian noise $n(t)$ with a known variance σ^2, so that, at $t = t_i$, we have a mixture

$$y_i(t) = u_i(t) + n(t) = V_i(t)\cos[2\pi f_i t + \theta_i(t)], \tag{11}$$

where $V_i \geq 0$ is a positive valued envelope with the Rice distribution and $|\theta_i| \leq \pi$ is the modulo 2π random phase[2]. Although the frequency f_i in the reflected pulses can be different, below we often let the frequencies be equal, by setting $f_k = f_0$. The instantaneous peak SNR in $y_i(t)$ (Fig. 1b) is calculated by

$$\gamma_i = \frac{S\beta^2(t_i)}{\sigma^2}. \tag{12}$$

Because of noise, the actual phase difference[3]

$$\bar{\Theta}_k = \vartheta_{2k} - \vartheta_{2k-1} = \psi_{2k-1} - \psi_{2k} \tag{13}$$

$$= \frac{4\pi}{v}[f_{2k-1}L_1 - f_{2k}L_2] \tag{14}$$

$$\cong -2\pi f_0 \Delta\tau_{(2k)(2k-1)}, \tag{15}$$

where $\vartheta_{2k-1} = \vartheta_1(t_{2k-1})$, $\vartheta_{2k} = \vartheta_2(t_{2k})$, $\psi_{2k-1} = \psi_1(t_{2k-1})$, and $\psi_{2k} = \psi_2(t_{2k})$ cannot be measured precisely and are estimated at the coherent receiver via the noisy phase difference $\theta_{2k} - \theta_{2k-1}$ as (3), using (1) or (2). Similarly, the time drift in $\bar{\Theta}_k$ is evaluated by

$$\bar{\Psi}_k = \bar{\Theta}_k - \bar{\Theta}_{k-1} \tag{16}$$

$$= -\psi_{2k} + \psi_{2k-1} + \psi_{2k-2} - \psi_{2k-3}. \tag{17}$$

So, instead of the actual angle $\bar{\Theta}_k$, the coherent receiver produces its random estimate $\hat{\Theta}_k$ and instead of $\bar{\Psi}_k$ we have $\hat{\Psi}_k$. Note that, in the ideal receiver, Θ_k and $\hat{\Theta}_k$ as well as Ψ_k and $\hat{\Psi}_k$ have the same distributions [11].

3. Probability density of the phase difference

Because both the received signal and noise induced by the receiver are essentially narrowband processes, the instantaneous phase θ_i in (11) has Bennett's conditional distribution

[2] Throughout the paper, we consider the modulo 2π phase and phase difference.

[3] For the sake of simplicity, we assume equal phases $\phi(t_{2k})$ and $\phi(t_{2k-1})$. It is important that a linearly drifting phase difference $\phi(t_{2k}) - \phi(t_{2k-1})$ does not affect distribution of Θ_k [8] and may be accounted as a regular error.

$$p(\theta_i \mid \gamma_i, \vartheta_i) = \frac{e^{-\gamma_i}}{2\pi} + \sqrt{\frac{\gamma_i}{\pi}} e^{-\gamma_i \sin^2 \tilde{\theta}_i} \Phi\left(\sqrt{2\gamma_i}\cos\tilde{\theta}_i\right)\cos\tilde{\theta}_i, \tag{18}$$

where $\tilde{\theta}_i = \theta_i - \vartheta_i$ and $\Phi(x) = \frac{1}{\sqrt{2\pi}}\int_{-\infty}^{x} e^{-t^2/2}\mathrm{d}t$ is the probability integral. It has been shown in [17, 13] that (18) is fundamental for the interrogating RF pulses of arbitrary waveforms and modulation laws.

Employing the maximum likelihood function approach, the coherent receiver produces an estimate $\hat{\theta}_i$ of θ_i [11]. Assuming in this paper an ideal receiver, we let $\hat{\theta}_i = \theta_i$. Provided (18), the pdf of the information bearing phase difference Θ_k can be found for equal and different SNRs in the pulses and we notice that the problem is akin to that in two channel phase systems.

3.1 Different SNRs in the RF pulses

Most generally, one can suppose that the SNRs in the reflected pulses are different, $\gamma_{2k-1} \neq \gamma_{2k}$, owing to design problems and the SAW attenuation with distance. The relevant conditional pdf was originally published by Tsvetnov in 1969 [16]. Independently, in 1981, Pawula presented an alternative formula [21] that soon after appeared in [18] in a simpler form of

$$p(\Theta_k \mid \gamma_{2k-1}, \gamma_{2k}, \bar{\Theta}_k) = \frac{e^{-\bar{\gamma}}}{2\pi}\left[\cosh\breve{\gamma} + \frac{1}{2}\int_0^{\pi}\left(\bar{\gamma}\sin y + \lambda\right)\cosh(\breve{\gamma}\cos y)\times e^{\lambda\sin y}\mathrm{d}y\right], \tag{19}$$

where $\bar{\gamma} = (\gamma_{2k-1} + \gamma_{2k})/2$, $\breve{\gamma} = (\gamma_{2k} - \gamma_{2k-1})/2$, $\xi = \arctan\frac{\breve{\gamma}}{\lambda}$, $\lambda = \sqrt{\gamma_{2k-1}\gamma_{2k}}\cos\tilde{\Theta}_k$, and $\tilde{\Theta}_k = \Theta_k - \bar{\Theta}_k$. An equivalence of the Tsvetnov and Pawula pdfs was shown in [22].

To avoid computational problems, Tsvetnov expended his pdf in [20] to the Fourier series

$$p(\Theta_k \mid \gamma_{2k-1}, \gamma_{2k}, \bar{\Theta}_k) = \frac{1}{2\pi} + \frac{1}{\pi}\sum_{n=1}^{N} c_n(\gamma_{2k-1}, \gamma_{2k})\cos n(\Theta_k - \bar{\Theta}_k), \tag{20}$$

where N is proportional to the maximum SNR in the pulses, $c_n(\gamma_{2k-1}, \gamma_{2k}) = c_n(\gamma_{2k-1})c_n(\gamma_{2k})$, and

$$c_n(\gamma_i) = \frac{\sqrt{\pi\gamma_i}}{2} e^{-\gamma_i/2}\left[I_{(n+1)/2}\left(\frac{\gamma_i}{2}\right) + I_{(n-1)/2}\left(\frac{\gamma_i}{2}\right)\right], \tag{21}$$

where $I_v(x)$ is the modified Bessel function of the first kind and fractional order v. The mean and mean square values associated with (20) have been found in [24] to be, respectively,

$$\left\langle \Theta_k \right\rangle = 2\sum_{n=1}^{N}\frac{(-1)^{n+1}}{n} c_n(\gamma_{2k-1}, \gamma_{2k})\sin n\bar{\Theta}_k, \tag{22}$$

$$\left\langle \Theta_k^2 \right\rangle = \frac{\pi^2}{3} + 4\sum_{n=1}^{N}\frac{(-1)^n}{n^2} c_n(\gamma_{2k-1}, \gamma_{2k})\cos n\bar{\Theta}_k. \tag{23}$$

3.2 Equal SNRs in the RF pulses

In a special case when the SNRs in the pulses ara supposed to be equal, $\bar{\gamma}_k = \gamma_{2k-1} = \gamma_{2k}$, the phase difference has the conditional Tsvetnov pdf [20]

$$p(\Theta_k \mid \bar{\gamma}_k, \bar{\Theta}_k) = \frac{e^{-\bar{\gamma}_k}}{2\pi}\left[1 + \int_0^{\pi/2} \left(\bar{\gamma}_k \cos z + \lambda_k\right) e^{\lambda_k \cos z} dz\right], \tag{24}$$

where $\lambda_k = \bar{\gamma}_k \cos \tilde{\Theta}_k$. Note that Tsvetnov published his pdf in the functional form. The integral equivalent (24) shown in [11] does not appear in Tsvetnov's works. It can be observed that, by equal SNRs, (19) becomes (24), although indirectly.

3.3 Probability density of the differential phase difference

It has been shown in [22] that the pdf of the differential phase difference (DPD) has two equivalent forms.

The first form of this pdf appears to be

$$\begin{aligned} p_\Psi &\triangleq p(\Psi_k \mid \gamma_{2k}, \gamma_{2k-1}, \gamma_{2k-2}, \gamma_{2k-3}, \bar{\Psi}_k) \\ &= \frac{e^{-\bar{\gamma}_1 - \bar{\gamma}_2}}{2\pi}\left[A + \frac{1}{4}\int_0^{\pi}\int_0^{\pi} \cosh(\bar{\gamma}_1 \cos x)\cosh(\bar{\gamma}_2 \cos y) F(x, y, \tilde{\Psi}_k) \mathrm{d}x\mathrm{d}y\right], \end{aligned} \tag{25}$$

where $\bar{\gamma}_1 = (\gamma_{2k-1} + \gamma_{2k})/2$, $\bar{\gamma}_2 = (\gamma_{2k-3} + \gamma_{2k-2})/2$,

$$\begin{aligned} F = &\left[\bar{\gamma}_1\bar{\gamma}_2 \sin x \sin y + \frac{1}{2}\sqrt{\gamma_{2k}\gamma_{2k-1}\gamma_{2k-2}\gamma_{2k-3}}\cos\tilde{\Psi}\right] I_0(a) \\ &+ \left[\bar{\gamma}_1\sqrt{\gamma_{2k-3}\gamma_{2k-2}}\cos(\tilde{\Psi} + \zeta)\sin x + \bar{\gamma}_2\sqrt{\gamma_{2k-1}\gamma_{2k}}\cos\zeta \sin y\right] I_1(a) \\ &+ \frac{1}{2} I_2(a)\sqrt{\gamma_{2k}\gamma_{2k-1}\gamma_{2k-2}\gamma_{2k-3}}\cos(\tilde{\Psi} + 2\zeta), \end{aligned} \tag{26}$$

$$\begin{aligned} a(x, y, \tilde{\Psi}) = \Big[&2\sqrt{\gamma_{2k}\gamma_{2k-1}\gamma_{2k-2}\gamma_{2k-3}}\sin x \sin y \cos\tilde{\Psi} \\ &+ \gamma_{2k-1}\gamma_{2k}\sin^2 x + \gamma_{2k-3}\gamma_{2k-2}\sin^2 y\Big]^{1/2}, \end{aligned} \tag{27}$$

$$\zeta(x, y, \tilde{\Psi}) = \begin{cases} \arctan(Q/I), & I \geq 0 \\ \arctan(Q/I) \pm \pi, & I < 0, \begin{cases} Q \geq 0 \\ Q < 0 \end{cases} \end{cases}, \tag{28}$$

$$Q = -\sqrt{\gamma_{2k-3}\gamma_{2k-2}}\sin y\tilde{\Psi}, \tag{29}$$

$$I = \sqrt{\gamma_{2k-1}\gamma_{2k}}\sin x + \sqrt{\gamma_{2k-3}\gamma_{2k-2}}\sin y\cos\tilde{\Psi}. \tag{30}$$

By changing the variables, namely by substituting sin x with x and sin y with y, the pdf transforms to its second equivalent form of

$$p_{\Psi}=\frac{e^{-\bar{\gamma}_1-\bar{\gamma}_2}}{2\pi}\left[A+\int_0^1\int_0^1\frac{\cosh(\breve{\gamma}_1\sqrt{1-x^2})\cosh(\breve{\gamma}_2\sqrt{1-y^2})}{\sqrt{(1-x^2)(1-y^2)}}\times G(x,y,\tilde{\Psi}_k)\mathrm{d}x\mathrm{d}y\right], \tag{31}$$

where

$$\begin{aligned}G=&\left[\bar{\gamma}_1\bar{\gamma}_2xy+\frac{1}{2}\sqrt{\gamma_{2k}\gamma_{2k-1}\gamma_{2k-2}\gamma_{2k-3}}\cos\tilde{\Psi}_k\right]I_0(b)\\&+\left[\bar{\gamma}_2\sqrt{\gamma_{2k-1}\gamma_{2k}}\,y\cos\zeta+\bar{\gamma}_1\sqrt{\gamma_{2k-3}\gamma_{2k-2}}\,x\cos(\tilde{\Psi}_k+\zeta)\right]\\&\times\ I_1(b)+\frac{1}{2}I_2(b)\sqrt{\gamma_{2k}\gamma_{2k-1}\gamma_{2k-2}\gamma_{2k-3}}\cos(\tilde{\Psi}_k+2\zeta),\end{aligned} \tag{32}$$

$$\begin{aligned}b(x,y,\tilde{\Psi}_k)=&\Big[2xy\sqrt{\gamma_{2k}\gamma_{2k-1}\gamma_{2k-2}\gamma_{2k-3}}\cos\tilde{\Psi}_k\\&+\gamma_{2k-1}\gamma_{2k}x^2+\gamma_{2k-3}\gamma_{2k-2}y^2\Big]^{1/2},\end{aligned} \tag{33}$$

and $\zeta(x,y,\tilde{\Psi})$ is given by (28) with $Q=-y\sqrt{\gamma_{2k-3}\gamma_{2k-2}}\sin\tilde{\Psi}_k$ and $I=x\sqrt{\gamma_{2k-1}\gamma_{2k}}+y\sqrt{\gamma_{2k-3}\gamma_{2k-2}}\cos\tilde{\Psi}_k$.

One may arrive at the conclusion that neither (25) nor (31) allow for further substantial simplifications and closed forms even in the special case of equal SNRs in the first and second pulses.

3.3.1 Equal SNRs in the first and second pulses

By letting $\gamma_1=\gamma_{2k-1}$ and $\gamma_2=\gamma_{2k}$, the pdf p_ψ attains the form shown in [22]

$$p_{\Psi}=\frac{e^{-2\bar{\gamma}}}{2\pi}\left[2e^{\breve{\gamma}}\cosh\breve{\gamma}-\cosh^2\breve{\gamma}+\int_0^1\int_0^1\frac{\cosh(\breve{\gamma}\sqrt{1-x^2})\cosh(\breve{\gamma}\sqrt{1-y^2})}{\sqrt{(1-x^2)(1-y^2)}}\times G(x,y,\tilde{\Psi}_k)\mathrm{d}x\mathrm{d}y\right], \tag{34}$$

where $\bar{\gamma}=(\gamma_2+\gamma_1)/2$, $\breve{\gamma}=(\gamma_2-\gamma_1)/2$,

$$\begin{aligned}G=&\left(\bar{\gamma}^2xy+\frac{\gamma_1\gamma_2}{2}\cos\tilde{\Psi}_k\right)I_0(b)+\bar{\gamma}\sqrt{\gamma_1\gamma_2}\left[y\cos\zeta+x\cos(\tilde{\Psi}_k+\zeta)\right]\\&\times I_1(b)+\frac{\gamma_1\gamma_2}{2}I_2(b)\cos(\tilde{\Psi}_k+2\zeta),\end{aligned} \tag{35}$$

$$b(x,y,\tilde{\Psi}_k)=\left[\gamma_1\gamma_2(x^2+2xy\cos\tilde{\Psi}_k+y^2)\right]^{1/2}, \tag{36}$$

and $\zeta(x,y,\tilde{\Psi}_k)$ is given by (28) with $Q=-y\sqrt{\gamma_1\gamma_2}\sin\tilde{\Psi}_k$ and $I=\sqrt{\gamma_1\gamma_2}(x+y\cos\tilde{\Psi}_k)$.

3.3.2 Equal SNRs in the pulses

For SAW sensors with closely placed reflectors, one may suppose that all of the received RF pulses have equal SNRs, $\gamma=\gamma_{2k-1}=\gamma_{2k}$. By setting $\bar{\gamma}=\gamma$ and $\breve{\gamma}=0$, substituting the

hyperbolic functions with the exponential ones, and providing the routine transformations, we arrive at the pdf originally derived in [25],

$$\begin{aligned} p_{\Psi} &= p(\Psi_k \mid \gamma, \bar{\Psi}_k) \\ &= \frac{2e^{-\gamma} - e^{-2\gamma}}{2\pi} + \frac{\gamma^2 e^{-2\gamma}}{2\pi} + \int_0^1 \int_0^1 \frac{\mathrm{d}x\mathrm{d}y}{\sqrt{(1-x^2)(1-y^2)}} \\ &\quad \times [E_1 I_0(\gamma E_2) + E_3 I_1(\gamma E_2)], \end{aligned} \tag{37}$$

where

$$E_1 = xy(1 + E_2^{-2}\sin^2\tilde{\Psi}) + \cos\tilde{\Psi}, \tag{38}$$

$$E_2 = \sqrt{x^2 + 2xy\cos\tilde{\Psi} + y^2}, \tag{39}$$

$$E_3 = (E_2\cos\tilde{\Psi} + 2xyE_2^{-2}\sin^2\tilde{\Psi})(1 - \gamma^{-1}E_2^{-2}). \tag{40}$$

Certainly, (37) can be used when there is no substantial difference in the RF pulses of the received burst, although (34) gives us a more realistic picture. Notwith-standing this fact, neither of the above discussed pdfs has engineering features. Below, we shall show that this disadvantage is efficiently circumvented with quite simple and reasonably accurate approximations.

4. Von-Mises/Tikhonov-based approximations

Observing the above-described probability densities of the phase difference and DPD, one can deduce they all these relations are not suitable for the engineering use and approximations having simpler forms would be more appropriate. It has been shown in [14] that efficient approximations can be found employing the von Mises/Tikhonov distribution known as circular normal distribution. The von Mises/Tikhonov pdf [15] is

$$p(\varphi) = \frac{1}{2\pi I_0(\alpha)} e^{\alpha\cos(\varphi - \varphi_0)}, \tag{41}$$

where $\alpha(\gamma)$ is the SNR-sensitive parameter, φ is the mod 2π variable phase, and φ_0 is some constant value. Commonly, (41) is used by the authors to approximate Bennett's pdf (18) for the instantaneous phase θ with the error of about 5% and $\alpha(\gamma)$ specified in the least mean squares (LMS) sense. Shmaliy showed in [14] that (41) fits better the phase difference pdf with equal SNRs allowing for the approximation error lesser 0.6%. Referring to this fact, below we give simple and reasonably accurate von Mises/Tikhonov-based distributions for the phase difference and DPD.

4.1 Phase difference

To fit the phase difference Θ_k with arbitrary SNRs, Tsvetnov proposed in [16] an approximation

$$p(\Theta_k \mid \bar{\gamma}_k, \bar{\Theta}_k) = \frac{1}{2\pi I_0(\bar{\gamma}_k)} e^{\bar{\gamma}_k\cos(\Theta_k - \bar{\Theta}_k)}, \tag{42}$$

where

$$\bar{\gamma}_k = \frac{2\gamma_{2k-1}\gamma_{2k}}{\gamma_{2k-1}+\gamma_{2k}}, \tag{43}$$

allowing for a maximum error of about 20%. Referring to [16], Shmaliy showed in [14] that (41) works out with a maximum error at $\gamma_{2k-1} = \gamma_{2k} \simeq 0.6$ of about 0.6% if to write

$$p(\Theta_k \mid \bar{\gamma}_k, \bar{\Theta}_k) = \frac{1}{2\pi I_0(\alpha_k)} e^{\alpha_k \cos(\Theta_k - \bar{\Theta}_k)} \tag{44}$$

and set

$$\alpha_k = \bar{\gamma}_k (1 + a e^{-b\bar{\gamma}_k}), \tag{45}$$

where a = 0.525 and b = 1.1503 are determined in the least mean squares (LMS) sense. With $\gamma_{2k-1} \neq \gamma_{2k}$, the error increases up to about 5 % with the SNRs difference tending toward infinity. The mean and mean square values associated with (44), for a fixed α_k, are, respectively,

$$\left\langle \Theta_k \right\rangle = 2\sum_{n=1}^{N} \frac{(-1)^{n+1}}{n} \varrho_{n0}(\alpha_k) \sin n\bar{\Theta}_k, \tag{46}$$

$$\left\langle \Theta_k^2 \right\rangle = \frac{\pi^2}{3} + 4\sum_{n=1}^{N} \frac{(-1)^n}{n^2} \varrho_{n0}(\alpha_k) \cos n\bar{\Theta}_k, \tag{47}$$

where N is proportional to the SNR and

$$\varrho_{ij}(x) = \frac{I_i(x)}{I_j(x)} \tag{48}$$

is a ratio of the modified Bessel functions of the first kind and integer order. It can be shown that, by zero and large SNRs, (44) becomes uniform and normal, respectively,

$$p(\Theta_k) = \frac{1}{2\pi}, \tag{49}$$

$$p(\Theta_k \mid \bar{\gamma}_k, \bar{\Theta}_k) = \sqrt{\frac{\bar{\gamma}_k}{2\pi}} e^{-\frac{\bar{\gamma}_k}{2}(\Theta_k - \bar{\Theta}_k)^2}, \tag{50}$$

having in the latter case (50) the variance $\sigma_\Theta^2 = 1/\bar{\gamma}_k$.

4.2 Differential phase difference

It has also been shown in [14] that, to fit Ψ_k, the following von Mises/Tikhonov- based approximations may be used with a maximum error of about 0.41 % at equal unit SNRs. For different and equal SNRs these pdfs are, respectively[4],

[4] (52) was originally derived in [17].

$$p(\Psi_k \mid \bar{\gamma}_{k-1}, \bar{\gamma}_k, \bar{\Psi}_k) = \frac{1}{2\pi} \frac{I_0(r_k)}{I_0(\alpha_{k-1}) I_0(\alpha_k)}, \tag{51}$$

$$p(\Psi_k \mid \bar{\gamma}_k, \bar{\Psi}_k) = \frac{1}{2\pi} \frac{I_0(r_{1k})}{I_0^2(\alpha_k)}, \tag{52}$$

where

$$r_k = \sqrt{\alpha_{k-1}^2 + 2\alpha_{k-1}\alpha_k \cos(\Psi_k - \bar{\Psi}_k) + \alpha_k^2},$$
$$r_{1k} = \alpha_k \sqrt{2[1 + \cos(\Psi_k - \bar{\Psi}_k)]}.$$

The mean and mean square values associated with (51) and (52) are, respectively,

$$\langle \Psi_k \rangle = 2 \sum_{n=1}^{N} \frac{(-1)^{n+1}}{n} \varrho_{n0}(\alpha_{k-1}, \alpha_k) \sin n\bar{\Psi}_k, \tag{53}$$

$$\langle \Psi_k^2 \rangle = \frac{\pi^2}{3} + 4 \sum_{n=1}^{N} \frac{(-1)^n}{n^2} \varrho_{n0}(\alpha_{k-1}, \alpha_k) \cos n\bar{\Psi}_k, \tag{54}$$

where $\varrho_{n0}(\alpha_{k-1}, \alpha_k) = \varrho_{n0}(\alpha_{k-1}) \varrho_{n0}(\alpha_k)$.
Several important limiting cases can now be distinguished.

4.2.1 Case 1: Large SNR in one of the signals

With $\bar{\gamma}_k \gg 1$ and $\bar{\gamma}_{k-1} \ll \bar{\gamma}_k$, the pdf (51) degenerates to the von Mises/Tikhonov density (41).

4.2.2 Case 2: One of the signals is a pure noise

Let $\bar{\gamma}_k = 0$ and $\bar{\gamma}_{k-1} \neq 0$. With $\bar{\gamma}_k = 0$, (51) transforms to the uniform density (49) disregarding the other SNR value. Therefore, (52) also becomes uniform.

4.2.3 Case 3: Large and equal SNRs in the vectors

With $1 \ll \bar{\gamma}_{k-1} = \bar{\gamma}_k$, the pdf (52) degenerates to the normal density

$$p(\Psi_k \mid \bar{\gamma}_k, \bar{\Psi}_k) \cong \sqrt{\frac{\bar{\gamma}_k}{4\pi}} e^{-\frac{\bar{\gamma}_k}{4}(\Psi_k - \bar{\Psi}_k)^2}, \tag{55}$$

in which the variance is $\sigma_\Psi^2 = 2 / \bar{\gamma}_k$.
As can be observed, all the von Mises/Tikhonov-based approximations have simple engineering forms allowing for small errors with typically near equal SNRs in the received SAW sensor pulses.

5. Errors in the phase difference estimates

To evaluate errors in the estimates of phase angles, let us assume that the actual phase difference between the received pulses of the SAW sensor is $\bar{\Theta}_k$. At the receiver, this

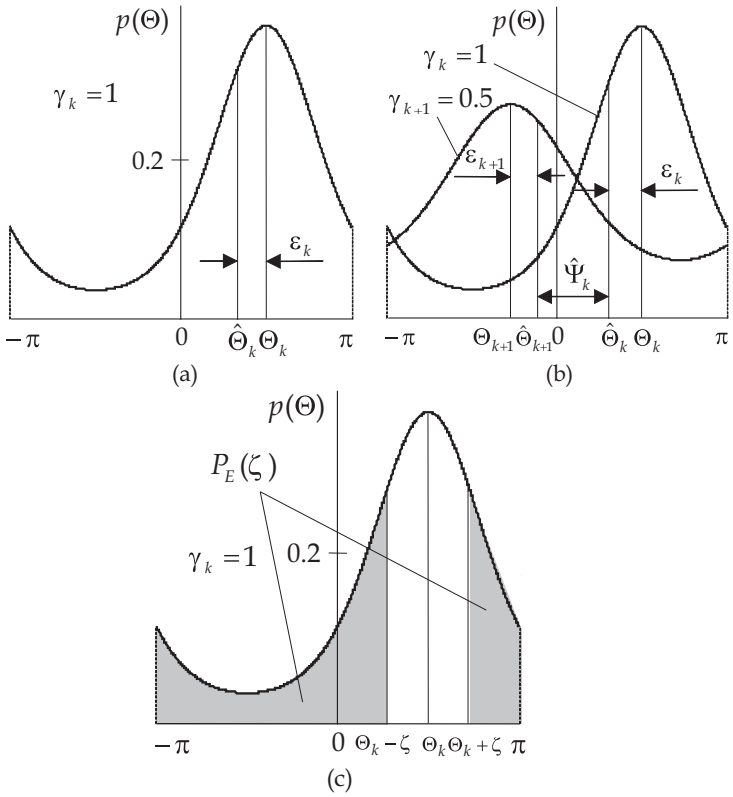

Fig. 2. Errors in passive SAW sensing with DPM and $\gamma_k = 1$: (a) instantaneous ϵ_k, (b) differential phase diversity $\hat{\Psi}_k$, and (c) error probability $P_E(\zeta)$ [25]. Note that, with $\gamma_k \gg 1$, the pdf tends to be normal and, by $\gamma_k \to 0$, it becomes uniform.

difference becomes noisy and is estimated as $\hat{\Theta}_k$ with the probability density (19) or (44). We thus have an estimate with the instantaneous error $\epsilon_k = \bar{\Theta}_k - \hat{\Theta}_k$. Figure 2a illustrates the estimate errors for the case of $\gamma_k = 1$, in which we recognize the mean error (bias) and the mean square error (MSE), respectively,

$$\langle \epsilon_k \rangle = \bar{\Theta}_k - \langle \hat{\Theta}_k \rangle, \tag{56}$$

$$\langle \epsilon_k^2 \rangle = \bar{\Theta}_k^2 - 2\bar{\Theta}_k \langle \hat{\Theta}_k \rangle + \langle \hat{\Theta}_k^2 \rangle. \tag{57}$$

When two neighboring values, $\hat{\Theta}_k$ and $\hat{\Theta}_{k+1}$, are unequal then the differential phase diversity $\hat{\Psi}_k$ occurs (Fig. 2b). If $\langle \hat{\Psi}_k \rangle = 0$, then the estimates $\hat{\Theta}_k$ are mutually unbiased. Otherwise, $\langle \hat{\Psi}_k \rangle$ causes a bias in the multiple DPM that may be associated with the sensor movement (Doppler effect).

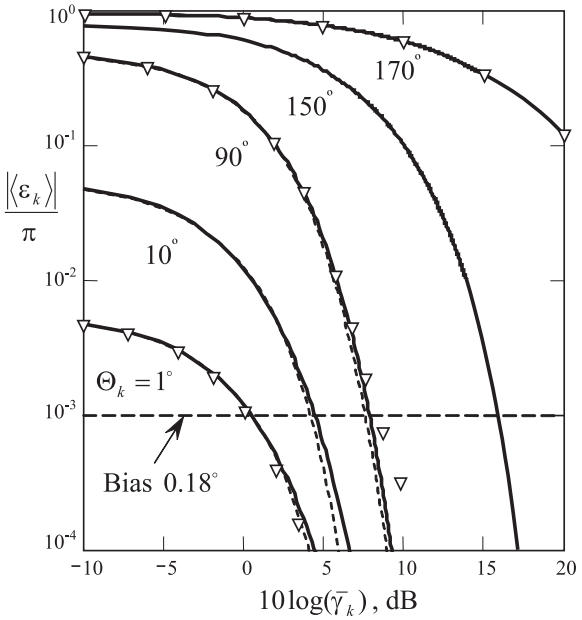

Fig. 3. Mean errors calculated for equal SNRs by (19) rigorously (bold) with c_n (21) and approximately (dashed) by (44) with ϱ_{n0} (48)[25].

5.1 Mean error

The mean error (bias) in the estimate can be evaluated if we test the rigorous and approximate distributions by (56). That gives us

$$\langle \epsilon_k \rangle = \bar{\Theta}_k - 2\sum_{n=1}^{N} \frac{(-1)^{n+1}}{n} A_n \sin n\bar{\Theta}_k , \tag{58}$$

where A_n is the amplitude of the Fourier series component. One must let $A_n = c_n(\gamma_{2k-1}, \gamma_{2k})$ as specified with (21) if the bias is calculated via the Tsvetnov/Pawula pdf (19). If the von Mises/Tikhonov-based approximating pdf (44) is used, then substitute A_n with $\varrho_{n0}(\alpha_k)$ specified with (48). Note that in each of these cases, the length N of the series is practically limited by the doubled maximum SNR in the pulses. Figure 3 exhibits $\langle \epsilon_k \rangle$ calculated rigorously, by c_n, and approximately, by ϱ_{n0}, for equal SNRs $\bar{\gamma}_k$. Here, triangle points represent simulation. It is seen that the approximation is accurate in a whole range of angles and SNRs.

5.2 Mean square error

Employing (57) and reasoning along similar lines, one can find the MSE in the estimate in the form of

$$\langle \epsilon_k^2 \rangle = \frac{\pi^2}{3} + \bar{\Theta}_k^2 + 4\sum_{n=1}^{N} \frac{(-1)^n}{n} A_n \left(\frac{1}{n} \cos n\bar{\Theta}_k + \bar{\Theta}_k \sin n\bar{\Theta}_k \right). \tag{59}$$

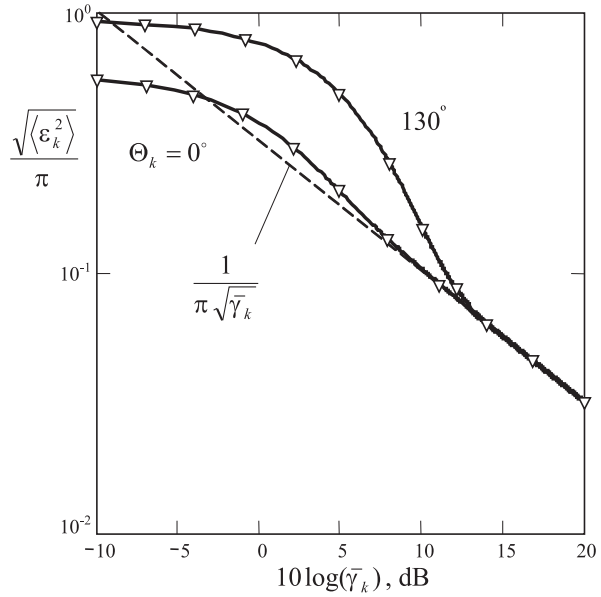

Fig. 4. Root MSEs calculated with equal SNRs. No visible error is observed between the rigorous estimate, by c_n, and approximate estimate, by ϱ_{n0}. The asymptotic behavior (61) is dashed [25].

It may also be calculated approximately in two important special cases:

- $\bar{\gamma}_k < 0$ dB, then

$$\left\langle \epsilon_k^2 \right\rangle \cong \frac{\pi^2}{3} + \bar{\Theta}_k^2 - \pi\bar{\gamma}_k e^{-\bar{\gamma}_k}\left(1 + \frac{\bar{\gamma}_k}{4} + \frac{\bar{\gamma}_k^2}{16}\right)^2 \left(\cos\bar{\Theta}_k + \bar{\Theta}_k \sin\bar{\Theta}_k\right) + \frac{\bar{\gamma}_k^2 e^{-\bar{\gamma}_k}}{16}\left(\frac{\bar{\gamma}_k}{3} + 2\right)^2 \left(\cos 2\bar{\Theta}_k + 2\bar{\Theta}_k \sin 2\bar{\Theta}_k\right), \tag{60}$$

- If $\bar{\gamma}_k > 13$ dB, then

$$\left\langle \epsilon_k^2 \right\rangle \cong \frac{1}{\bar{\gamma}_k}. \tag{61}$$

Figure 4 sketches the root MSE (RMSE) calculated rigorously, by c_n, and approximately, by ϱn_0, for equal SNRs, $\bar{\gamma}_k$. One can observe that there is no visible difference between two curves and thus the von Mises/Tikhonov approximation is highly accurate. Furthermore, by large SNR $\bar{\gamma}_k > 13$ dB, both curves converge to the asymptotic line given by (61).

5.3 Error variance and Cramér-Rao lower bound

A measure of noise in the estimate is the variance calculated for a single DPM by

$$\sigma_{\Theta k}^2 = \langle \hat{\Theta}_k^2 \rangle - \langle \hat{\Theta}_k \rangle^2. \tag{62}$$

With multiple DPM, the variance is often substituted with the Cramér-Rao lower bound (CRLB) having approximate, although typically simple representations. Supposing that the measurement vector **x** is formed with N readings as $\mathbf{x} = [x_0\, x_1 \ldots x_{N-1}]^T$ with the uncorrelated phase difference components x_k having equal SNRs, $\alpha_k = \alpha$, and actual phase difference $\bar{\Theta}$, the likelihood function can be written as

$$p(\mathbf{x};\bar{\Theta}) = \frac{1}{[2\pi I_0(\alpha)]^N} e^{\alpha \sum_{k=0}^{N-1} \cos(x_k - \bar{\Theta})}. \tag{63}$$

Accordingly, the CRLB calculates

$$\sigma_\Theta^2 \geq \frac{1}{-\langle \frac{\partial^2}{\partial \bar{\Theta}^2} ln p(\mathbf{x};\bar{\Theta}) \rangle}$$

$$= \frac{1}{\alpha N r \cos(\bar{\Theta} - \phi)}, \tag{64}$$

where $r = \sqrt{\bar{x}_c^2 + \bar{x}_s^2}$, $\phi = arctan \frac{\bar{x}_s}{\bar{x}_c}$, $\bar{x}_c = \frac{1}{N} \sum_{k=0}^{N-1} \cos x_k$, and $\bar{x}_s = \frac{1}{N} \sum_{k=0}^{N-1} \sin x_k$. It is seen that large N causes a substantial decrease in the estimate variance. It can also be shown that, for single DPM, the CRLB reduces to

$$\sigma_\Theta^2 \geq \frac{1}{\alpha \cos(\bar{\Theta} - x_0)}, \tag{65}$$

where x_0 may be assumed to be either $\langle \Theta \rangle$ or Θ_0.

Figure 5 illustrates this analysis. We first notice that the von Mises/Tikhonov approximation does not produce a visible error, like in Fig. 4. By (65) and $x_0 = \Theta_0$, The CRLB holds true for all angles and traces below the asymptotic line (61) owing to the function (45) (see the case of $\Theta_k = 0^o$). With $x_0 = \langle \Theta \rangle$, (65) produces more realistic values if SNRs > 0 dB and too large values with SNRs < 0 dB that may not be appropriate in applications (see the case of $\Theta_k = 130^o$).

6. Error probability for the estimate to exceed a threshold

The error probability P_E of passive remote SAW sensing is the conditional probability $P(\zeta \leq | \bar{\Theta}_k - \hat{\Theta}_k \| \gamma_{2k-1}, \gamma_{2k})$ for the error in the estimate of the phase difference between two pulses $| \bar{\Theta}_k - \hat{\Theta}_k |$ to exceed a threshold ζ. The P_E is represented by the shadowed area in Fig. 2c. Its quantity does not depend on $\bar{\Theta}_k$ and can be approximately estimated by

$$P_E(\zeta \mid \gamma_{2k-1}, \gamma_{2k}) = 1 - \frac{\zeta}{\pi} - \frac{2}{\pi} \sum_{n=1}^{N} \frac{1}{n} A_n \sin n\zeta, \tag{66}$$

$$\cong 1 - \frac{\zeta}{\pi} \left(1 + 2 \sum_{n=1}^{N} A_n \right), \quad \zeta \ll \pi, \tag{67}$$

$$\cong 1 - \frac{\zeta}{\pi} \left(1 + 2 \sum_{n=1}^{N} e^{-n^2 \frac{\gamma_{k+}}{2\gamma_{k\times}^2}} \right), \quad \zeta \ll \pi, \quad 1 \ll \gamma_i. \tag{68}$$

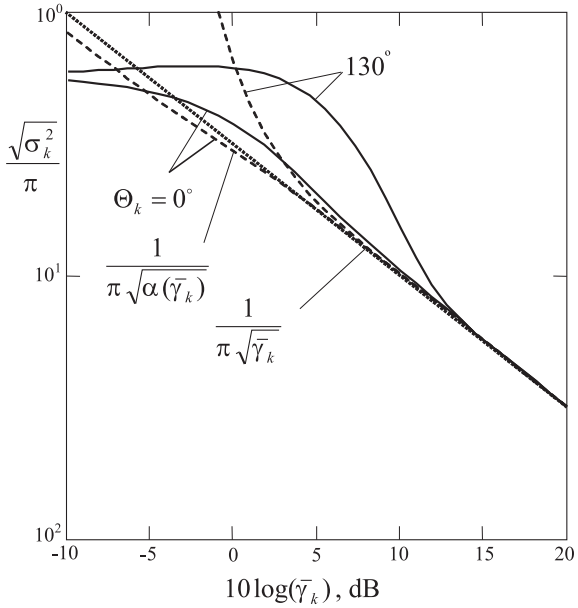

Fig. 5. Variance estimate with single DPM for two angles Θ = 0° and Θ = 130°: rigorous (bold), asymptotic (dotted), and CRLBs (dashed) [24].

where $A_n = c_n(\gamma_{2k-1}, \gamma_{2k})$ is specified with (21), if the bias is calculated via the Tsvetnov/Pawula pdf (19), and A_n must be substituted with $\varrho_{n0}(\alpha_k)$, if the von Mises/Tikhonov-based approximating pdf (44) is used.

The estimate of P_E is akin to that in the calculus of the conditional symbol error (SER) for the differentially coherent detection in digital communication channels with M-ary phase difference shift keying (MPDSK).We exploit it below to find approximate solutions for remote SAW sensing.

6.1 Approximate estimates for equal SNRs

Since $P_E(\zeta)$ is $\bar{\Theta}_k$ invariant, one can set $\bar{\Theta}_k = 0$ and go to the symmetric pdf $p(\Theta \mid \bar{\gamma}_k)$. The error probability can thus be calculated for a threshold ζ to range from 0 to π as [11]

$$P_E(\zeta \mid \bar{\gamma}_k) = 2\int_{\zeta}^{\pi} p(\Theta_k \mid \bar{\gamma}_k) d\Theta_k \tag{69}$$

$$= \frac{e^{-\bar{\gamma}_k}}{\pi} \sin\zeta \int_0^{\pi/2} \frac{e^{\bar{\gamma}_k \cos\zeta \cos t}}{1 - \cos\zeta \cos t} dt. \tag{70}$$

A similar formula employed in [18] is known as the conditional SER,

$$P_E(M \mid \bar{\gamma}_k) = 2\int_{\pi/M}^{\pi} p(\Theta_k \mid \bar{\gamma}_k) \mathrm{d}\Theta_k, \tag{71}$$

where M is an integer but may be arbitrary in a common case. By $M = \pi/\zeta$, (71) becomes (70) and we notice that (71) was performed in [18] in the integral form that, by symmetry of the integrand, simplifies to (70).
Alternatively, one can substitute (44) into (69) and arrive at the familiar von Mises/Tikhonov approximation

$$P_{ET}(\zeta \mid \overline{\gamma}_k) = \frac{1}{\pi I_0(\alpha_k)} \int_{\zeta}^{\pi} e^{\alpha_k \cos x} dx. \tag{72}$$

By employing the Fourier series analysis, one can also transform (72) to the computationally more preferable form of

$$P_{ET}(\zeta \mid \overline{\gamma}_k) = 1 - \frac{\zeta}{\pi} - \frac{2}{\pi} \sum_{n=1}^{N} \frac{1}{n} \varrho_{n0}(\alpha_k) \sin n\zeta. \tag{73}$$

Observing the above-given results concerning the error probability, several special cases can be distinguished.

6.1.1 Large and equal SNRs

It has been shown in [11] that large SNRs allow for the approximation of (69) by

$$P_E(\zeta \mid \overline{\gamma}_k \gg 1) \cong 2Q\left(\zeta \sqrt{\overline{\gamma}_k}\right), \tag{74}$$

where $Q(x) = \frac{1}{2}$ erfc $(\frac{x}{\sqrt{2}})$ is the Gauss Q-function and erfc(x) is the complimentary error function. Several other approximate solutions found by Fleck and Trabka, Arthurs and Dym, Bussgang and Leiter, and Salz and Stein for $\pi/\zeta > 2$ where reported in [18]. These solutions are, respectively,

$$P_E(\zeta \mid \overline{\gamma}_k \gg 1) \cong \operatorname{erfc} X + \frac{X e^{-X^2}}{4\sqrt{\pi}(\overline{\gamma}_k + 0.125)}, \tag{75}$$

$$\cong \operatorname{erfc}\left(\sqrt{\overline{\gamma}_k} \sin \frac{\zeta}{\sqrt{2}}\right), \tag{76}$$

$$\cong \operatorname{erfc}\left(\frac{\overline{\gamma}_k}{\sqrt{1 + 2\overline{\gamma}_k}} \sin \zeta\right), \tag{77}$$

$$\cong \sqrt{\frac{1 + \cos\zeta}{2\cos\zeta}} \operatorname{erfc} X, \tag{78}$$

where $X(\zeta, \overline{\gamma}_k) = \sqrt{\overline{\gamma}_k (1 - \cos\zeta)}$. In turn, (44) becomes normal (50) with large SNRs, and one more approximation can be proposed for this case, namely

$$P_E(\zeta \mid \overline{\gamma}_k \gg 1) \cong 2Q\left(\zeta \sqrt{\overline{\gamma}_k}\right) - 2Q\left(\pi \sqrt{\overline{\gamma}_k}\right). \tag{79}$$

It has been shown in [14] that, among all other known approximations, the von Mises/Tikhonov-based one (72) is most accurate.

6.1.2 Low and equal SNRs

The case of SNR $\cong$ 0 dB allows for an asymptotic form of (70), by letting $e^x \cong 1-x$ and then integrating; that is,

$$P_E(\zeta \mid \overline{\gamma}_k \le 1) \cong \frac{2}{\pi}\arctan\frac{\sin\zeta}{1-\cos\zeta} - \frac{\overline{\gamma}_k}{2}\sin\zeta . \tag{80}$$

It turns out, however, that the inaccuracy of (80) is larger than that produced by (73), if we set $N = 2$. The latter approximation is given by

$$P_{ET}(\zeta \mid \overline{\gamma}_k \cong 1) \cong 1 - \frac{\zeta}{\pi} - \frac{2}{\pi}\varrho_{10}(\alpha_k)\left[1+\varrho_{21}(\alpha_k)\cos\zeta\right]\sin\zeta \tag{81}$$

$$= 1 - \frac{\zeta}{\pi} - \frac{2}{\pi}\varrho_{10}(\alpha_k)\left(1-\frac{2}{\alpha_k}\cos\zeta\right)\sin\zeta - \frac{1}{\pi}\sin 2\zeta . \tag{82}$$

6.1.3 Very low and equal SNRs

Let us finally consider the case of $\overline{\gamma}_k \ll 1$. With such values of $\overline{\gamma}_k$, (80) simplifies to

$$P_E(\zeta \mid \overline{\gamma}_k \ll 1) \cong \frac{2}{\pi}\arctan\frac{\sin\zeta}{1-\cos\zeta} \tag{83}$$

and, because $\varrho_{10}(x \ll 1) \cong 4x/(x^2+8)$, the approximation (82) becomes

$$P_{ET}(\zeta \mid \overline{\gamma}_k < 1) \cong 1 - \frac{\zeta}{\pi} - \frac{2}{\pi}\varrho_{10}(\alpha_k)\sin\zeta \tag{84}$$

$$\cong 1 - \frac{\zeta}{\pi} - \frac{8\alpha_k}{\pi(\alpha_k^2+8)}\sin\zeta . \tag{85}$$

Again, we notice that (80) is not a rival here, being still lesser accurate, and, as a matter of fact, we note that only with SNR < –20 dB the approximate functions (83)-(85) trace along the same trajectory.

Figure 6 illustrates the rigorous, by (70), and approximate, by (72), calculation of the error probability for equal SNRs and different values of the threshold. A splendid property of the von Misis/Tikhonov-based approximations is indicated instantly: the error is negligible in the whole range of angles with arbitrary values of SNRs.

7. Phase difference drift rate

A measure D of the drift rate of the phase difference Θ_k in the received RF pulse- burst has three critical applications: 1) It represents the drift rate error when the burst is used to increase the SNR in the received signal [7]; 2) When the SAW sensor is intended to measure a physical quantity, then D characterizes speed of change of this quantity; and 3) If the SAW reader system measures velocity of a moving object, then D gives a measure of acceleration. In applications, of interest are the mean value $\langle D \rangle$ and variance σ_D^2 of the drift rate.

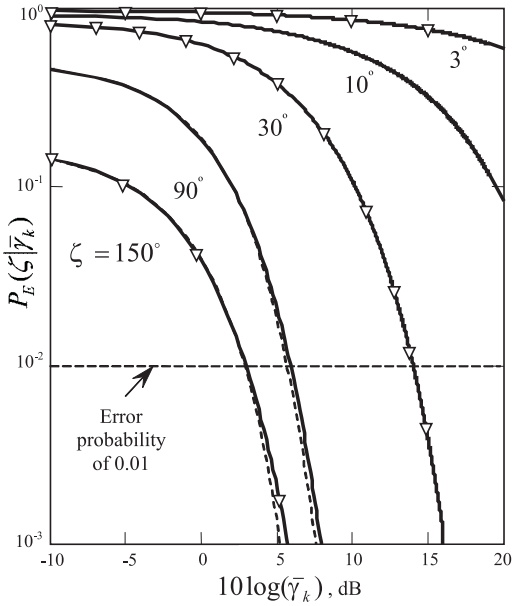

Fig. 6. Error probability for equal SNRs: rigorous (bold), by (70), and approximated by von Mises/Tikhonov's distribution (dashed), by (72) [25].

7.1 Mean drift rate

The mean drift rate $\langle D\rangle$ can be evaluated employing both (51) and the mean value $\langle \Psi_k\rangle$ given in [11] as in the following,

$$\langle D\rangle = \frac{\langle \Psi_k\rangle}{T} \tag{86}$$

$$= \frac{1}{T}\int_{-\pi}^{\pi} \Psi_k \overline{p}(\Psi_k \,|\, \gamma_{2k}, \gamma_{2k-1}, \gamma_{2k-2}, \gamma_{2k-3}, \tilde{\Psi}_k) \mathrm{d}\Psi_k \tag{87}$$

$$\cong \frac{2}{T}\sum_{n=1}^{N} \frac{(-1)^{n+1}}{n} \frac{I_n(\alpha_1)}{I_0(\alpha_1)} \frac{I_n(\alpha_2)}{I_0(\alpha_2)} \sin n\bar{\Psi}_k, \tag{88}$$

where a reasonable series length is limited with $N \geq 2 \max\ \bar{\gamma}_{1,2}$ [3]. The estimate of $\langle D\rangle$ can be found by averaging $\hat{\Psi}_k$ at the coherent receiver as

$$\langle \hat{D}\rangle = \frac{1}{TK}\sum_{k=1}^{K} \hat{\Psi}_k. \tag{89}$$

Example 1: Burst length vs. the drift rate [25]. Consider a passive SAW sensor of temperature [10] operating at the frequency f_0 = 2.45 GHz with the temperature sensitivities of the delay time difference S_t = 0.017 ns/K and phase difference $S_p = 2\pi f_0 S_t$ = 0.262 rad/K. Suppose that the temperature rate at the sensor substrate is 1 K per 10 sec; that is

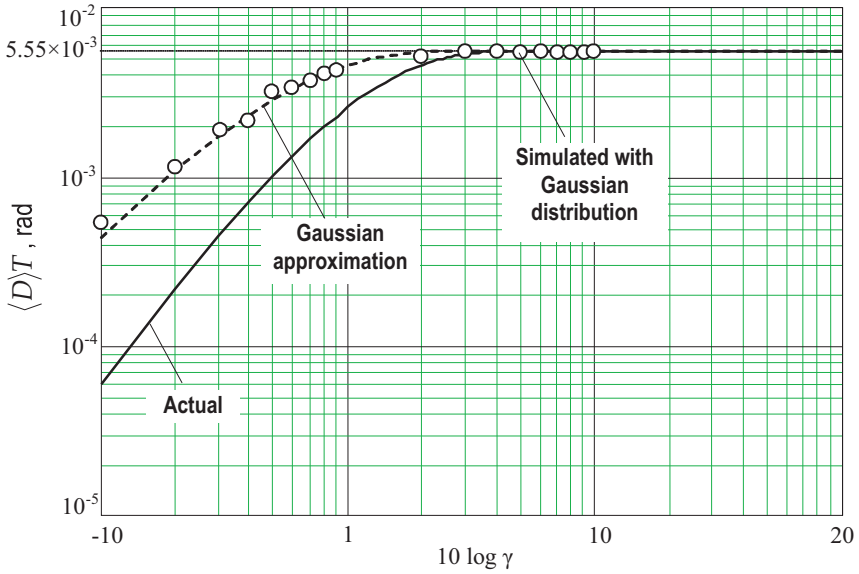

Fig. 7. The mean drift rate $\langle D\rangle$ for $\bar{\Psi} = 5.55 \times 10^{-3}$ rad: actual, by (88); Gaussian approximation; and simulation with Gaussian distribution, using (89) [25].

γ	$\lvert\bar{\Psi}\rvert$, rad					
	0.1π	0.3π	0.5π	0.7π	0.8π	0.9π
dB	> 4	> 5	> 7	> 11	> 13	> 21

Table 1. Allowed γ for Accurate Estimation of $\langle D\rangle$ with Different $\bar{\Psi}$

$R_t = 10^{-10}$ K/ns. The phase difference mean drift rate is thus $\langle D\rangle = S_p R_t = 2.62\times10^{-11}$ rad/ns. The sensor is interrogated with the pulse-burst of K pulses and period T. During the burst length $L = KT$, temperature is changed at $\Delta T = R_t L$ K and the phase difference at $\Delta\Theta = \langle D\rangle L$ rad. For the allowed error of $\epsilon = 0.1^o$ in the temperature range of $T_r = 300^o$, the mean phase error is $\epsilon_p = \pi\epsilon / T_r = 1.047 \times 10^{-3}$ rad. By $\Delta\Theta = \epsilon_p$, the pulse-burst length is thus limited with $L \le \frac{\pi\epsilon}{\langle D\rangle T_r}\times 10^{-9} = 0.04\,\text{sec}$.

Example 2: Effect of the SNR on the mean drift rate [25]. Figure 7 shows effect of the SNR, by its equal values in each of the pulses, on $\langle D\rangle$ for $\bar{\Psi} = 5.55 \times 10^{-3}$ rad. Actual values are calculated by (88) for $\gamma \le 20$ and by (55) when $\gamma > 20$. Supposing that Ψ the Gaussian pdf (55) over all values of γ, we arrive at an approximation (dashed). For the latter case, the process was simulated and $\langle D\rangle$ calculated numerically (circles), by (89). As can be seen, the approximation errors practically vanish when γ exceeds 4 dB. Otherwise, bias occurs in the estimate. Table 1 gives the relevant values for $\bar{\Psi}$ ranging from 0.1π to 0.9π. A simple measure of accuracy used here is when the exact and approximate values become visually indistinguishable.

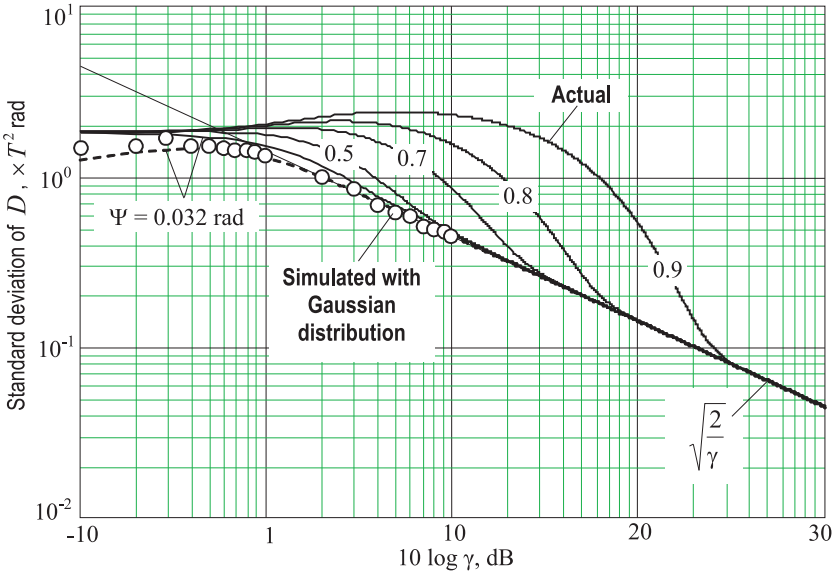

Fig. 8. The standard deviation $\sqrt{\sigma_D^2}$ for different $\bar{\Psi}$: actual (bold), by (90); Gaussian approximation (dashed) for $\bar{\Psi}$ = 0.032 rad; and simulation with Gaussian distribution, using (91).

γ	$\lvert\bar{\Psi}\rvert$, rad					
	0.1π	0.3π	0.5π	0.7π	0.8π	0.9π
dB	> 8	> 9	> 10	> 13	> 18	> 23

Table 2. Allowed γ for Accurate Evaluation of σ_D^2 with Different $\bar{\Psi}$

7.2 Drift rate variance

The phase difference drift rate variance can be represented, using (88), via the mean square value found in [11] to be [26]

$$\begin{aligned}\sigma_D^2 &= \frac{\left\langle \Psi_k^2 \right\rangle}{T^2} - \langle D \rangle^2 \\ &= \frac{1}{T^2}\left[\frac{\pi^2}{3} + 4\sum_{n=1}^{N}\frac{(-1)^n}{n^2}\frac{I_n(\alpha_1)}{I_0(\alpha_1)}\frac{I_n(\alpha_2)}{I_0(\alpha_2)}\cos n\bar{\Psi}_k\right] - \langle D \rangle^2\end{aligned} \tag{90}$$

and its estimate obtained by averaging as

$$\hat{\sigma}_D^2 = \frac{1}{TK}\sum_{k=1}^{K}(\hat{\Psi}_k - \langle D \rangle)^2 . \tag{91}$$

Figure 8 sketches the standard deviation $\sqrt{\sigma_D^2}$ evaluated by (90) and (91) for different values of $\bar{\Psi}$. Along, we show the estimates (dashed) and simulated values calculated by

(91) for $\bar{\Psi}$ = 0.032 rad assuming Gaussian approximation (55). For the comparison with the mean drift rate (Table 1), Table 2 gives minimum values of γ, for several $\bar{\Psi}$, allowing for accurate evaluation of σ_D^2. An important inference follows instantly. For the sake of minimum errors, the SNR in the pulses must be obtained larger than 23 dB for $\bar{\Psi}$ ranging from -0.9π to 0.9π. We notice that similar values were found in [3] and [14] for the phase difference Θ. An analysis shows that the CRLB cannot be found for multiple DPM in simple functions and the best candidate for the estimate of σ_D^2 still remains (91).

8. Error probability for the drift rate to exceed a threshold

In applications, the phase difference drift rate is often required to range below some allowed value. The relevant error probability P_E can be characterized by the probability for the DPD to exceed a threshold ζ. Because the pdf of the modulo 2π angular measure is 2π-periodical, the P_E is commonly ascertained by setting $\bar{\Psi}_k = 0$. Using (51), we thus have

$$P_E \triangleq P_E(\zeta \mid \bar{\gamma}_1, \bar{\gamma}_2)$$

$$= 2\int_{\zeta}^{\pi} \bar{p}(\Psi_k \mid \bar{\gamma}_1, \bar{\gamma}_2)\mathrm{d}\Psi_k \tag{92}$$

$$= \frac{1}{\pi I_0(\alpha_1) I_0(\alpha_2)} \int_{\zeta}^{\pi} I_0\left(\sqrt{\alpha_1^2 + 2\alpha_1\alpha_2 \cos z + \alpha_2^2}\right)\mathrm{d}z. \tag{93}$$

Expanding the integrand in (93) to the Fourier series

$$I_0\left(\sqrt{\alpha_1^2 + 2\alpha_1\alpha_2 \cos z + \alpha_2^2}\right) = \sum_{n=0}^{\infty} \epsilon_n I_n(\alpha_1) I_n(\alpha_2) \cos nz,$$

where $\epsilon_0 = 1$ and $\epsilon_{n>0} = 2$, brings (93) to several useful estimates

$$P_E = \sum_{n=0}^{\infty} \frac{\epsilon_n}{\pi n} \frac{I_n(\alpha_1)}{I_0(\alpha_1)} \frac{I_n(\alpha_2)}{I_0(\alpha_2)} \left(\sin n\pi - \sin n\zeta\right) \tag{94}$$

$$\cong 1 - \frac{\zeta}{\pi}\left[1 + 2\sum_{n=1}^{N} \frac{I_n(\alpha_1)}{I_0(\alpha_1)} \frac{I_n(\alpha_2)}{I_0(\alpha_2)} \frac{\sin n\zeta}{n\zeta}\right] \tag{95}$$

$$\cong 1 - \frac{\zeta}{\pi}\left[1 + 2\sum_{n=1}^{N} \frac{I_n(\alpha_1)}{I_0(\alpha_1)} \frac{I_n(\alpha_2)}{I_0(\alpha_2)}\right], \zeta \ll \pi, \tag{96}$$

$$\cong 1 - \frac{\zeta}{\pi}\left(1 + 2N\right), \quad \zeta \ll \pi, \quad 1 \ll \bar{\gamma}_{1,2}, \tag{97}$$

$$\leq 1 - \frac{\zeta}{\pi}\left(1 + 4\max \bar{\gamma}_{1,2}\right), \zeta \ll \pi, 1 \ll \bar{\gamma}_{1,2}. \tag{98}$$

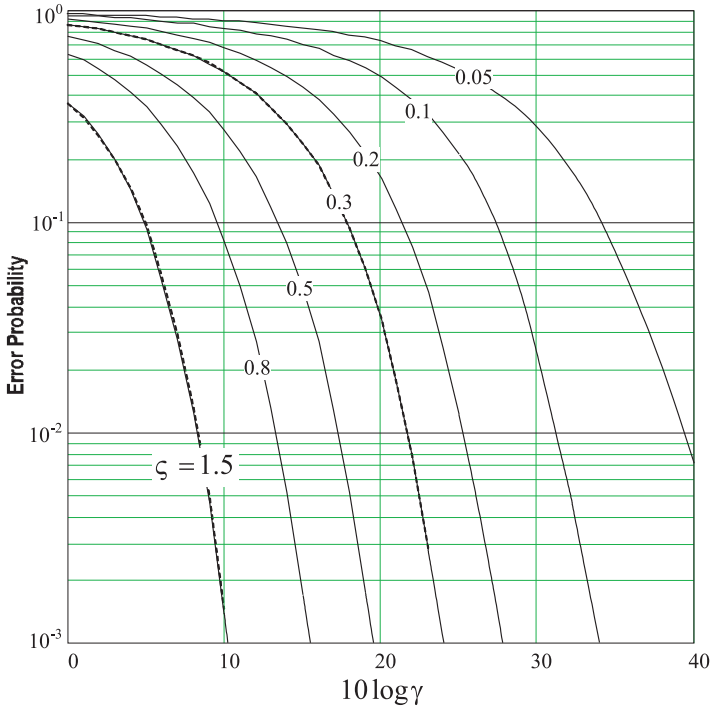

Fig. 9. Error probability of the drift rate to exceed a limit ζ with equal SNRs in the pulses: rigorous (dashed), by (37), and approximate (bold), by (95).

Figure 9 illustrates the error probability calculated rigorously (dashed), by (37) and (92), and approximately (bold), by (95) for equal SNRs in the pulses. One infers that the approximation error is negligibly small in the whole range of angular measures.

9. Conclusions

This Chapter gives a statistical analysis of errors in passive remote wireless surface acoustic wave sensing. By using the relations discussed, one can design the sensor reader system in an optimal way from the standpoint of maximum accuracy in measurement and minimum energy in the interrogating pulse. We were concerned with both rigorous and approximate estimates of the phase difference errors. It was shown that the rigorous pdfs cannot be represented in closed forms. In turn, the von Mises/Tikhonov-based densities are simple and reasonably accurate that makes them very attractive for engineering applications.

10. References

[1] Bulst, W.-E.; Fischerauer, G. & Reindl, L. (2001). State of the art in wireless sensing with surface acoustic waves. *IEEE Trans. on Industrial Electronics*, Vol. 48, No. 2, (April 2001)(265-271), ISSN 0278-0046.

[2] EerNisse, E.P. & Wiggins, R. B. (2001) Review of thickness-shear mode quartz resonator sensors for temperature and pressure, *IEEE Sensors J.*, Vol. 1, No. 1, (June 2001)(79-87), ISSN 1530-437X.

[3] Shmaliy, Y.S. (2000) Toward resonator anharmonic sensors for precision crystal oscillators: A Gaussian approach, *IEEE Trans. on Ultrason., Ferroel., and Freq. Contr.*, Vol. 47, No. 2, (Mar. 2000)(379-389), ISSN 0885-3010.

[4] Vig, J. R. (2001) Temperature-insensitive dual-mode resonant sensors – a review, *IEEE Sensors J.*, Vol. 1, No. 1, (June 2001)(62-68), ISSN 1530-437X.

[5] Schmidt, F.; Sczesny, O.; Ruppel, C. & Mágoni, V. (1996) Wireless interrogator system for SAW-Identification-Marks and SAW-Sensor components, *Proc. Int. Freq. Contr. Symp.*, pp. 208-215, ISBN 0-7803-3309-8, Hilton Hawaiian Village, June 1996, IEEE, Honolulu.

[6] Scholl, G.; Schmidt, F.; Ostertag, T.; Reindl, L.; Scherr, H. &Wolff, U. (1998) Wireless passive SAWsensor systems for industrial and domestic applications, *Proc. Int. Freq. Contr. Symp.*, pp. 595-601, ISBN 0-7803-4373-5, Ritz-Carlton Hotel, May 1998, IEEE, Pasadena.

[7] Pohl, A. A review of wireless SAW sensors, *IEEE Trans. on Ultrason, Ferroelect. and Freq. Contr.*, Vol. 47, No. 2, (Mar. 2000)(317-332), ISSN 0885-3010.

[8] Scheiblhofer, S.; Schuster, S. & Stelzer, A. 'Modeling and performance analysis of SAW reader systems for delay-line sensors, *IEEE Trans. Ultrason. Ferroel. Freq. Contr.*, Vol. 56, No. 10, (Oct. 2009)(2292-2303), ISSN 0885-3010.

[9] Shmaliy, Y. S. (2006) *Continuous-Time Signals*, Springer, ISBN-10 1-4020- 4817-3, Dordrecht.

[10] Reindl, L. M. & Shrena, I. M. Wireless Measurement of Temperature Using Surface Acoustic Waves Sensors, *IEEE Trans. on Ultrason, Ferroelect. And Freq. Contr.*, Vol. 51, No. 11, (Nov. 2004)(1457-1463), ISSN 0885-3010.

[11] Shmaliy, Y. S. Limiting phase errors of passive wireless SAW sensing with differential measurement, *IEEE Sensors J.*, Vol. 4, No. 6, (Dec. 2004)(819- 827), ISSN 1530-437X.

[12] Shmaliy, Y. S. On the multivariate conditional probability density of a vector perturbed by Gaussian noise, *IEEE Trans. Inform. Theory*, Vol. 53, No. 12, (Dec. 2007)(4792-4797), ISSN 0018-9448.

[13] Shmaliy, Y. S. Probability density of the phase of a random RF pulse in the presence of Gaussian noise, *Int. J. Electron. Commun.*, Vol. 63, No. 1, (Jan. 2009)(15-23), ISSN 1434-8411.

[14] Shmaliy, Y. S. Von Mises/Thkhonov-based distributions for systems with differential phase measurement, *Signal Process.*, Vol. 85, No. 4, (Apr. 2005)(693-703), ISSN 0165-1684.

[15] Tikhonov, V. I. The effect of noise on phase-lock oscillation operation, *Automatika i Telemekhanika*, Vol. 20, No. 9, (Sep. 1959)(1188-1196).

[16] Tsvetnov, V. V. Unconditional statistical characteristics of signals and uncorrelated Gaussian noises in two-channel phase systems, *Radiotekh. I Elektronika*, Vol. XIV, No. 12, (Dec. 1969)(2147-2159).

[17] Shmaliy, Y. S.; Shkvarko, Y. V.; Torres-Cisnerros, M.; Rojas-Laguna, R. & Ibarra-Manzano, O. A stochastic analysis of an anharmonic sensor phase response, *IEEE Sensors J.*, Vol. 3, No. 2, (Apr. 2003)(158-163), ISSN 1530- 437X.

[18] Pawula, R. F.; Rice, S. O. & Roberts, J. H. Distribution of the phase angle between two vectors perturbed by Gaussian noise, *IEEE Trans. Comm.*, Vol. COM-30, No. 8 (Aug. 1982)(1828-1841), ISSN 0090-6778.

[19] Bennett, W. R. Methods of solving noise problems, *Proc. IRE*, Vol. 44, No. 5, (May 1956)(609-638).

[20] Tsvetnov, V. V. Statistical properties of signals and noises in two-channel phase systems, *Radiotekh.*, Vol. 12, No. 5, (May 1957)(12-29).

[21] Pawula, R. F. On the theory of error rates for narrow-band digital FM, *IEEE Trans. Comm.*, Vol. COM-29, No. 11, (Nov. 1981)(1634-1643), ISSN 0090- 6778.

[22] Shmaliy Y. S. & Shmaliy, O.Y. Probability density of the differential phase difference in applications to passive wireless surface acoustic wave sensing, *Int. J. Electron Commun.*, Vol. 63, No. 1, (Jan. 2009)(623{631), ISSN 1434-8411.

[23] Karpov, A. F. Parameter estimation of the distribution function of a radio signal phase, *Radioelectron. and Commun. Systems*, Vol. 26, No. 7, (Jul. 1983)(23-29).

[24] Shmaliy, Y. S.; Ibarra-Manzano, O.; Andrade-Lucio, J. & Rojas-Laguna, R. Approximate estimates of limiting errors of passive wireless SAW sensing with DPM, *IEEE Trans. on Ultrason., Ferroel., Freq. Control*, Vol. 52, No. 10, (Oct. 2005)(1797{1805), ISSN 0885-3010.

[25] Shmaliy, Y. S.; Shmaliy, O.Y. & Ibarra-Manzano, O. Drift errors in passive remote wireless SAW sensing with multiple DPM, *IEEE Sensors J.*, Vol. 9, No. 7, (Jul. 2009)(774-781), ISSN 1530-437X.

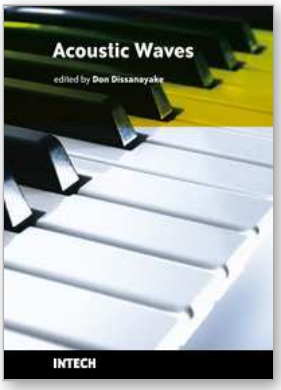

Acoustic Waves

Edited by Don Dissanayake

ISBN 978-953-307-111-4
Hard cover, 434 pages
Publisher Sciyo
Published online 28, September, 2010
Published in print edition September, 2010

SAW devices are widely used in multitude of device concepts mainly in MEMS and communication electronics. As such, SAW based micro sensors, actuators and communication electronic devices are well known applications of SAW technology. For example, SAW based passive micro sensors are capable of measuring physical properties such as temperature, pressure, variation in chemical properties, and SAW based communication devices perform a range of signal processing functions, such as delay lines, filters, resonators, pulse compressors, and convolvers. In recent decades, SAW based low-powered actuators and microfluidic devices have significantly added a new dimension to SAW technology. This book consists of 20 exciting chapters composed by researchers and engineers active in the field of SAW technology, biomedical and other related engineering disciplines. The topics range from basic SAW theory, materials and phenomena to advanced applications such as sensors actuators, and communication systems. As such, in addition to theoretical analysis and numerical modelling such as Finite Element Modelling (FEM) and Finite Difference Methods (FDM) of SAW devices, SAW based actuators and micro motors, and SAW based micro sensors are some of the exciting applications presented in this book. This collection of up-to-date information and research outcomes on SAW technology will be of great interest, not only to all those working in SAW based technology, but also to many more who stand to benefit from an insight into the rich opportunities that this technology has to offer, especially to develop advanced, low-powered biomedical implants and passive communication devices.

InTech Europe
University Campus STeP Ri
Slavka Krautzeka 83/A

InTech China
Unit 405, Office Block, Hotel Equatorial Shanghai
No.65, Yan An Road (West), Shanghai, 200040, China

51000 Rijeka, Croatia
Phone: +385 (51) 770 447
Fax: +385 (51) 686 166
www.intechopen.com

中国上海市延安西路65号上海国际贵都大饭店办公楼405单元
Phone: +86-21-62489820
Fax: +86-21-62489821